Supporting Information for

A New Signal Self-enhancement Photoelectrochemical Immunosensor without Addition Sacrificial Agent in Solution Based on Ag_2S/CuS/α-Fe_2O_3 n-p-n Heterostructure Films

Min Chen, Cun Wang, Fangjing Mo, Hui Meng, Yingzi Fu*

Key Laboratory of Luminescent and Real-Time Analytical Chemistry (Southwest University), Ministry of Education, School of Chemistry and Chemical Engineering, Southwest University, Chongqing 400715, China

List of Contents:

* Corresponding author: *Yingzi Fu*

Tel: +86-023-68252277

E-mail address: fyzc@swu.edu.cn

1. Reagents and apparatus

Cupric nitrate ($Cu(NO_3)_2$, 99.99%), silver nitrate ($AgNO_3$, 99.99%), sodium sulfide nonahydrate ($Na_2S·9H_2O$, 99.99%), ferric trichloride ($FeCl_3$, 99.99%), KCl (99.5%) and thioglycollic acid (TGA) were bought from the Chemical Reagent Co. (Chongqing, China).α-fetoprotein (AFP), carcinoembryonic antigen (CEA), prostate-specific antigen (PSA), prostate specific antibody (anti-PSA, unconjugated, designated as Ab1), N-Hydroxysuccinimide (NHS), 1-(3-Dimethylaminopropyl)-3-ethylcarbodiimide hydrochloride (EDC), L-cysteine (cys, 99%), Chloroauric acid ($HAuCl_4·4H_2O$, 99%), bovine serum albumin (BSA, ≥98%), acetonitrile (99%), ferrocene (99%), ascorbic acid (AA, 99%), sodium citrate (99%), tetrabutylammonium hexafluorophosphate ($TBAPF_6$, 98%) were purchased from J&k Chemical Co. (Beijing, China). Phosphate buffer saline (PBS, 0.1mol·L^{-1}) at various pH values were prepared by mixing the different ratio stock solutions of Na_2HPO_4 and KH_2PO_4 containing 0.1 mol·L^{-1} KCl as supporting electrolyte. 5 mmol·L^{-1} $[Fe(CN)_6]^{3-/4-}$ solution was composed of $K_4Fe(CN)_6$ and $K_3Fe(CN)_6$ (0.1 mol·L^{-1} PBS, pH 7.4). Healthy human serum samples were obtained from the Ninth People's Hospital of Chongqing, China. All reagents were analytical grade and used as received without further purification. The experimental water was double distilled (18.2 MΩ·cm).

Electrochemical measurements were performed on CHI 604D electrochemical workstation (Shanghai Chenhua Instruments Co., China), and PEC experiments were carried out at CHI 440A electrochemical workstation (Shanghai Chenhua Instruments Co., China) configured with PEAC 200A (Tianjin Ai Da Hengsheng Technology Co., Ltd., China) for visible-light irradiation. A three-electrode system was used to investigate the redox behaviors, which was composed of a glassy carbon electrode (GCE, Φ = 4.0 mm) as the working electrode, an Ag/AgCl (sat. KCl) as the reference electrode and a platinum

wire as the counter electrode. The UV-Vis spectra were recorded with a UV-2600 UV/Vis spectrophotometer (Shimadzu, Japan). Scanning electron microscopy (SEM) images and energy dispersive spectra (EDS) were acquired on a field emission SEM (ZEISS, Germany). The Fourier transform infrared spectra (FTIR) were obtained from Fourier Transform Infrared Spectrometer (PerkinElmer, USA). X-ray photoelectron spectroscopy (XPS) measurements were performed by an Axis Ultra spectrometer (Kratos Analytical Ltd., Japan) and the binding energy was calibrated by the O 1s peak at 532.4 eV and the C 1s peak at 284.8 eV. JEM 1200EX transmission electron microscopy (TEM, Tokyo, Japan) was applied to characterize the morphology and structure of the materials involved in this work. Electrochemical impedance spectroscopy (EIS) and Cyclic voltammetry (CV) measurements were carried out with a CHI 604 D electrochemistry workstation (Shanghai Chenhua Instruments Co, China) in 3.0 mL of 5 mmol·L^{-1} $[Fe(CN)_6]^{3-/4-}$. All measurements were carried out at the room temperature 25.0 ± 0.5°C.

2. Solvothermal synthesis of α-Fe_2O_3 NPs

The α-Fe_2O_3 NPs were synthesized according to Reference 1. In a typical synthesis, 2.16 g $FeCl_3 \cdot 6H_2O$ was dissolved in 40 mL ethylene glycol with stirring for 40 min. 3.6 g sodium acetate and 0.5 g trisodium citrate were introduced into the solution at an interval of 20 min and vigorously mixed for 1 h. The homogenous solution was then transferred into a 100 mL Teflon lined autoclave and was placed at 180°C for 18 h. The resultant brown to black magnetic precipitate (α-Fe_2O_3) was purified under external magnetic field using ethanol/Milli Q water.

3. Synthesis of CuS NPs

The CuS NPs were prepared by the hydrothermal method according to Reference 2 with a slight modification. Initially, 145 mg L-cysteine was dissolved in 36 mL water, 3 mL $CuCl_2$ solution (0.1 $mol \cdot L^{-1}$) was dropwise added to the suspension over 20 min. Subsequently, the reaction solution was stirred for 30 min before it was transferred to a 50 mL Teflon-lined stainless steel autoclave and maintained at 160 °C for 12 h. The obtained product was washed three times with water and ethanol, and dried at 60 °C overnight.

4. Preparation of different Au NPs

Citrate–Au NPs Briefly, according to Reference 3, 1 mL of 1 wt. % solution of $HAuCl_4$ was mixed with 99 mL of water. Then 2.5 mL 1 wt. % sodium citrate solution was added quickly under boiling and stirring. When the solution changed to wine red, the heat source was removed and stored at 4 °C after cooling to room temperature.

SO_3^{2-}-Au NPs 300 μL of 0.1 % chlorauric acid solution was added in water to form 30 mL solution, while the solution was got boiling with heating reflux, 1 % L-cysteine 30 μL was quickly added, stirring vigorously and continuing to heat for 3 min, the solution was removed from heat, cooled to room temperature. At the beginning, the color of the solution changed from dark grey to purple red, and finally to pink, meaning the Au NPs coated by SO_3^{2-} solution were obtained.

Cysteine-Au NPs Cysteine-coated Au NPs were obtained by ligand exchange in two ways. Firstly, 30 μL 1 % L-cysteine was added slowly into citrate–Au NPs solution, the color of the solution changed from wine red to purple, and the Au NPs capped by cysteine were obtained and recorded as Cys-Au NPs(i). Another kind of cysteine-Au NPs (Cys- Au NPs(ii)) were obtained by adding 30 μL L-cysteine into SO_3^{2-}-Au NPs solution.

5. Fabrication of different Au NPs@Ab2

SO_3^{2-}–Au NPs@Ab2 1 mL SO_3^{2-}–Au NPs (0.5 mg·mL^{-1}) were activated by the addition of EDC (100 μL, 20 mg·mL^{-1}) and NHS solution (100 μL, 10 mg·mL^{-1}). Subsequently, 2 mL of Ab2 solution (0.1 mg·mL^{-1}) was added, shaken gently overnight at 4°C. After centrifugation and washing with PBS three times, the bioconjugates (SO_3^{2-}–Au NPs@Ab2) were obtained by suspending in 2 mL of PBS (0.1 mol·L^{-1}, pH 7.4), and then reserved at 4°C for subsequent use.

Citrate–Au NPs@Ab2, Cys–Au NPs(i)@Ab2 and Cys–Au NPs(ii)@Ab2 They were obtained by similar experiment operations as the controls.

6. Immunoreaction and measurement procedure

All electrochemical measurements were carried out using three-electrode system at room temperature. EIS was used to study the preparation process of the BSA/anti-PSA/Ag_2S/CuS/α-Fe_2O_3/GCE in 5 mmol·L^{-1} $[Fe(CN)_6]^{3-/4-}$. CHI 440A electrochemical workstation configured external LED lamp with the output power about 14 mW·cm^{-2} was invited to conduct PEC measurements of the proposed electrodes. The detection was carried in 5 mL PBS (0.1 mol·L^{-1}, pH 7.4).

7. EIS performances of the stepwise modified electrodes

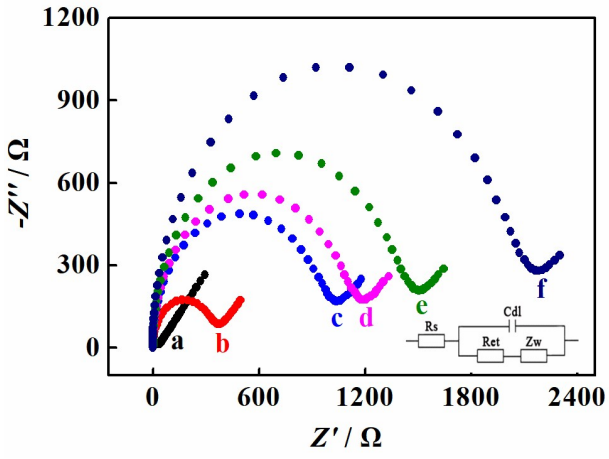

Fig.S1. Nyquist diagrams of EIS recorded from 0.01 Hz to 100 kHz for at (a) bare GCE, (b) α-Fe_2O_3/GCE, (c) CuS/α-Fe_2O_3/GCE, (d) Ag_2S/CuS/α-Fe_2O_3/GCE, (e) anti-PSA/Ag_2S/CuS/ α-Fe_2O_3/GCE, (f) BSA/anti-PSA/Ag_2S/CuS/ α-Fe_2O_3 /GCE in 5 mL 5 mmol·L^{-1} $[Fe(CN)_6]^{3-/4}$ (pH 7.4).

8. The elemental mappings of n-p-n composite

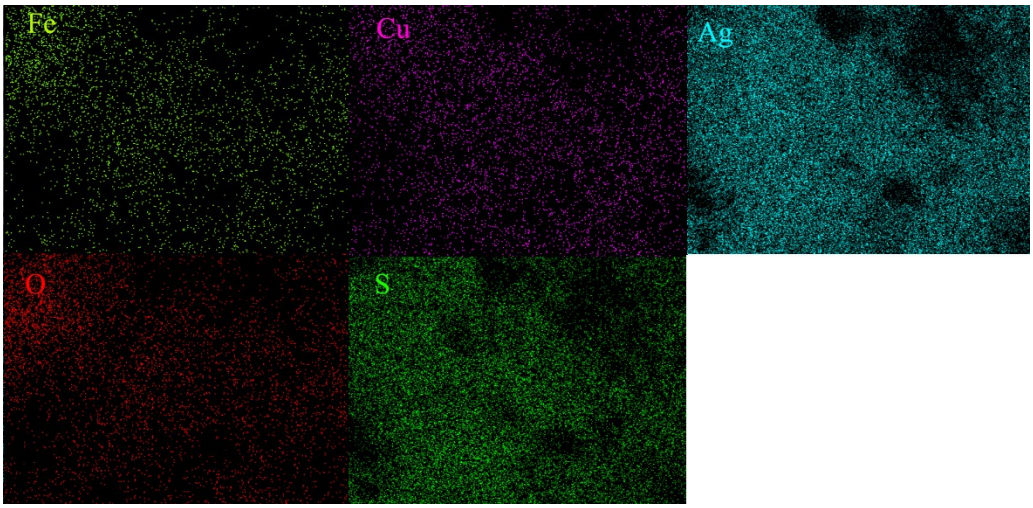

Fig.S2. The elemental mappings of Ag_2S/CuS/α-Fe_2O_3 n-p-n composite.

9. FTIR and EDX Characteristics of different materials

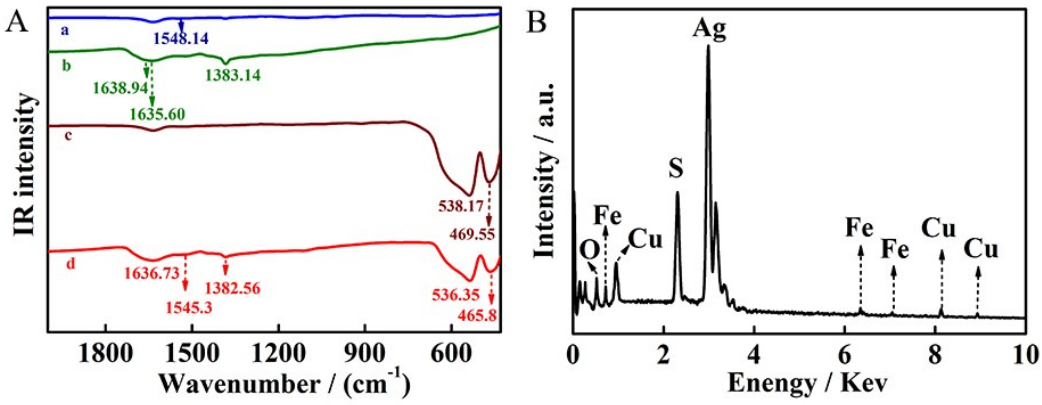

Fig.S3. (A) FTIR profiles of different materials (a) Ag_2S, (b) CuS, (c)α-Fe_2O_3 and (d) Ag_2S/CuS/α-Fe_2O_3. (B) EDX spectrum of Ag_2S/CuS/α-Fe_2O_3 film.

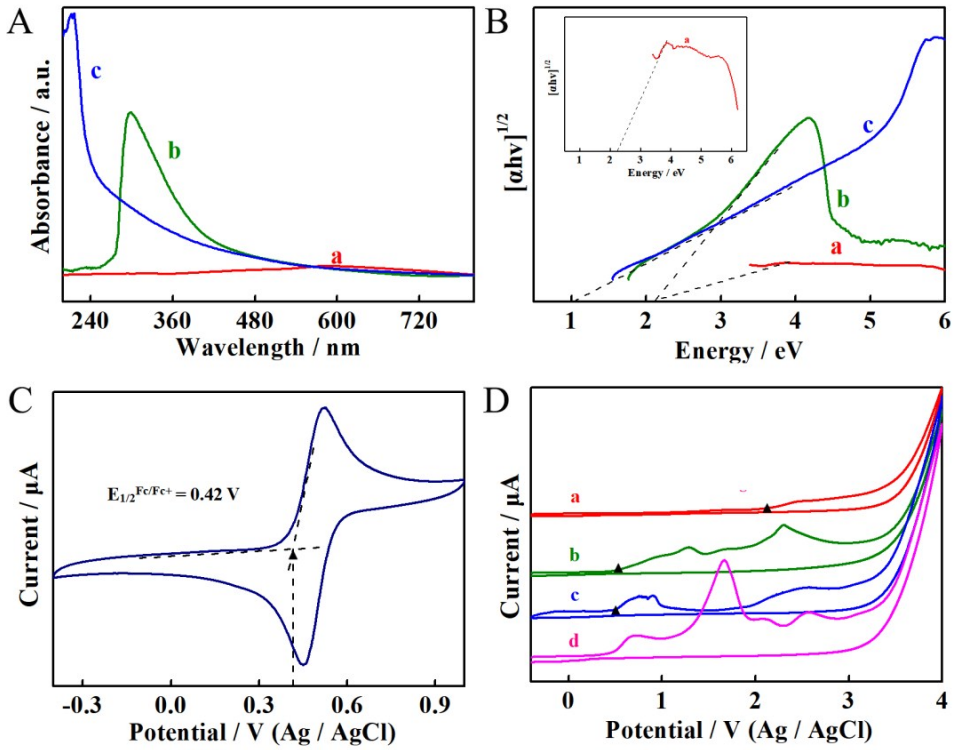

10. Band-gap determination of α-Fe_2O_3, CuS and Ag_2S

Fig.S4. (A) UV−vis spectra and (B) Tauc plots of indirect transitions: α-Fe_2O_3, CuS and Ag_2S. (C) Cyclic voltammograms (CVs) of bare GCE in a deoxygenated anhydrous acetonitrile solution containing 0.10 mol·L^{-1} tetrabutylammonium hexafluorophosphate ($TBAPF_6$) and 0.5 mmol·L^{-1} ferrocene (Fc) at a scan rate of 50 mV·s^{-1}. (D) CVs of α-Fe_2O_3/GCE, CuS/GCE, Ag_2S/GCE, and Ag_2S/CuS/α-Fe_2O_3/GCE as the working electrodes in 0.10 mol·L^{-1} $TBAP_6$ solutions in the same conditions at scan rate of 50 mV·s^{-1}. E_{ox} was calculated from tangents of the oxidation peaks of the species.

The energy band gaps of as-prepared Ag_2S, CuS, α-Fe_2O_3 were obtained by equation 1:

$$\alpha h\upsilon = B(h\upsilon - Eg)^{n/2} \quad (1)$$

where α, h and υ are absorption coefficient, Planck constant and light frequency, respectively; Eg and B are band gap energy and constant, respectively. Depending on being a direct or indirect bad gap semiconductor, the n value is 1 or 4, respectively.[4] From the extrapolation of the linear part of the plot of $(\alpha h\upsilon)^{(1/2)}$ versus ($h\upsilon$) (Fig. C) corresponding to each of the Ag_2S, CuS, α-Fe_2O_3, their corresponding band gaps (Eg) were determined to be 1.0, 2.2 and 2.2 eV, respectively.

The positions of the conduction band (CB) and valence band (VB) edges of the constituents of the Ag_2S/GCE, CuS/GCE, α-Fe_2O_3/GCE were estimated by calculating their electron affinity (EA) and ionization potential (IP) by using the following equations (2-3).[5] The energy levels of them can be gained by counting its lowest unoccupied molecular orbital (LUMO) and highest occupied molecular orbital (HOMO) by using the equations (4-5).

$$IP = -(4.80 - E_{1/2}^{Fc/Fc+} + E_{ox}) \quad (2)$$

$$EA = IP + Eg \quad (3)$$

$$E_{HOMO} = -(4.80 - E_{1/2}^{Fc/Fc+} + E_{ox}) \quad (4)$$

$$E_{LUMO} = E_{HOMO} + Eg \quad (5)$$

$E_{1/2}^{Fc/Fc+}$ is the formal potential of Fc/Fc^+, E_{ox} is the oxidation initiation potential. Potentials were calibrated with the ferrocene/ferrocenium (Fc/Fc^+) couple, and the potential of Fc/Fc^+ had an absolute energy level of 4.80 eV to vacuum. As shown in Fig. S3c, $E_{1/2}^{Fc/Fc+}$ was located at +0.42 V, with the use of bare GCE and scan rate of 50 $mV \cdot s^{-1}$ in 0.5 $mmol \cdot L^{-1}$ Fc solution. The CB/VB was thus determined as −4.38 eV/−6.58 eV for α-Fe_2O_3, −2.76 eV/−4.96 eV for CuS, and −3.93 eV/−4.93 eV for Ag_2S. These values

would be helpful for understanding the PEC behaviors of the designed n-p-n heterojunctions.

11. Optimization experiments

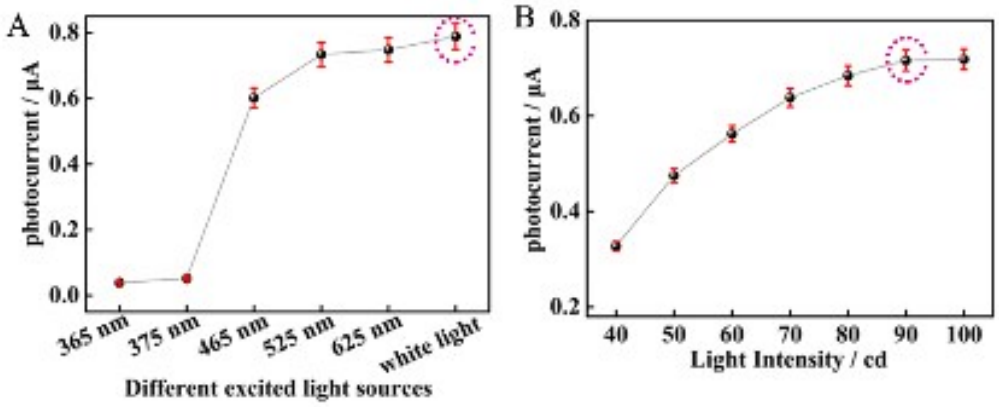

Fig.S5. PEC signal of immunosensors under the different wavelengths of excitation lights (A) and the white light intensity (B).

12. PEC signal of different sensors immune responses

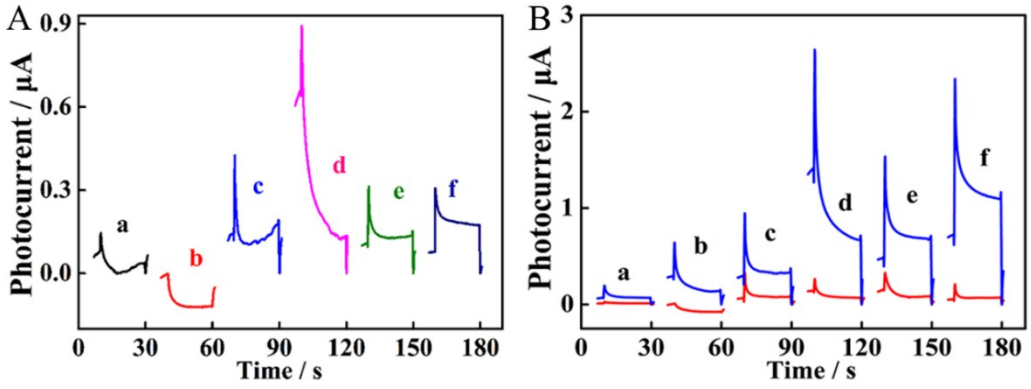

Fig.S6. (A) PEC signal of (a) α-Fe_2O_3, (b) CuS, (c) Ag_2S, (d) CuS/α-Fe_2O_3, (e) Ag_2S/CuS and (f) Ag_2S/CuS/α-Fe_2O_3 modified on the GCE in PBS solution. (B) The PEC

immunosensor made from (a) BSA/anti-PSA/α-Fe_2O_3/GCE, (b) BSA/anti-PSA/CuS/GCE, (c) BSA/anti-PSA/Ag_2S/GCE, (d) BSA/anti-PSA/CuS/α-Fe_2O_3/GCE, (e) BSA/anti-PSA/Ag_2S/CuS/GCEand (f) BSA/anti-PSA/Ag_2S/CuS/α-Fe_2O_3/GCE.

Table S1. PEC responses of different immunosensors before and after immune reaction in PBS solution

Immunosensors	I(blank) (/μA)	I(1ng·mL^{-1} PSA) (/μA)	I(1ng·mL^{-1} PSA)/ I(blank)
BSA/anti-PSA/α-Fe_2O_3/GCE	0.0124	0.0692	5.60
BSA/anti-PSA/CuS/GCE	-0.0041	0.141	-
BSA/anti-PSA/Ag_2S/GCE	0.0803	0.331	4.13
BSA/anti-PSA/CuS/α-Fe_2O_3/GCE	0.0692	0.668	9.68
BSA/anti-PSA/Ag_2S/CuS/GCE	0.0871	0.703	8.05
BSA/anti-PSA/Ag_2S/CuS/α-Fe_2O_3/GCE	0.0714	1.102	15.41

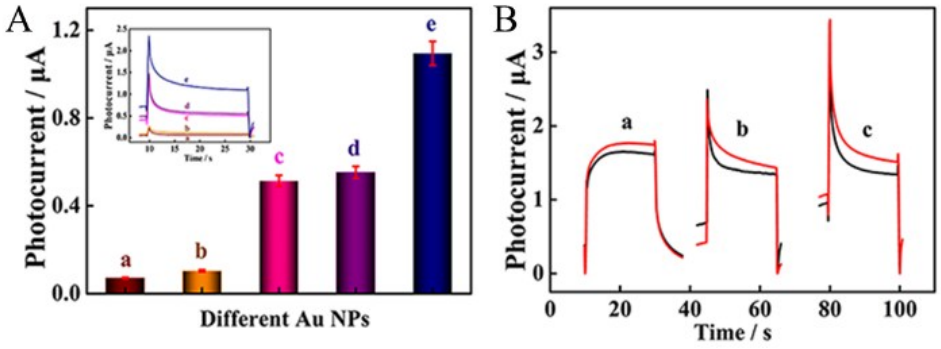

Fig.S7. (A) photoelectric self-enhancement of different Au NPs@Ab2 towards 1ng·mL^{-1} PSA: (a) blank, (b) Citrate–AuNPs, (c) Cys–AuNPs(i), (d) Cys–Au NPs(ii), (e) SO_3^{2-}–Au NPs. (B) PEC signals of SO_3^{2-}–Au NPs@Ab2 in 1ng·mL^{-1} PSA (0.1mol·L^{-1} PBS, pH 7.4) with addition 10 mmol·L^{-1} (a) L-cysteine, (b) AA and (c) sodium sulfite.

13. Selectivity of the PEC immunosensors

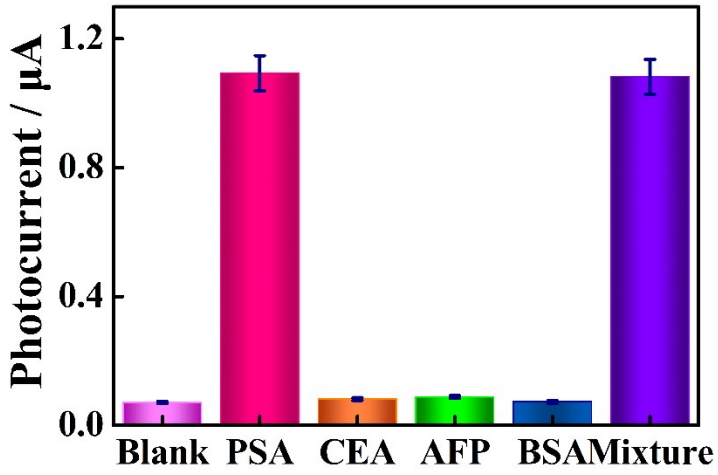

Fig.S8. Selectivity of the PEC immunosensor in blank, PSA, CEA, AFP, 1wt.% BSA and the mixture (PSA, CEA, AFP and 1wt.% BSA) respectively, the concentrations are all 1.0 pg·mL^{-1}

14. Detection of PSA in diluted human serum samples.

The applicability of the designed biosensors had been assessed for real samples. Before testing, the healthy human serum samples were centrifuged, and the supernatant was diluted 50 times (0.1 mol·L^{-1} PBS, pH 7.4). The standard addition method was used to measure the different concentrations of PSA. It obtains acceptable performance in real samples for the spike recoveries ranged from 98.7% to 100.4% (table S2).

Table S2. Recovery tests for PSA in human serum samples (n=6)

Sample number	Added (fg·mL^{-1})	Found (fg·mL^{-1})	Recovery (%)
1	15.0	14.8	98.7
2	85.0	85.2	100.2
3	600.0	602.5	100.4

15. Stability of the PEC immunosensor

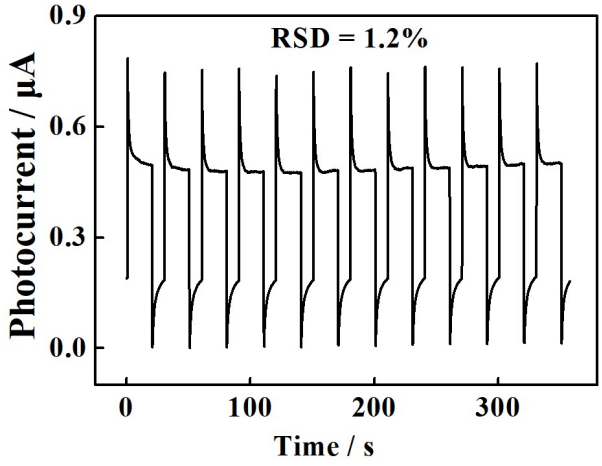

Fig.S9. Stability of the PEC immunosensor in 100 fg·mL^{-1} PSA.

16. Comparison of various methods for PSA activity assay

Table S3. Comparison of various methods for PSA activity assay

Methods	Linear range (ng·mL^{-1})	Detection limit (fg·mL^{-1})	References
Fluorescence	2.0×10^{-1}–1.2×10	6.0 ×10^{4}	6
Fluorescence	1.0×10^{-4}– 1.0×10^{-1}	3.0 ×10	7
Electrochemiluminescence	1.0×10^{-2} –5.0×10	3.0 ×10^{3}	8
Differential pulse voltammetric	2.0×10^{-3} –4.0×10	1.0 ×10^{3}	9
Field-effect transistor	1.0×10^{-1} –1.0	1.0 ×10^{2}	10
Surface-enhanced Raman scattering	1.0×10^{-3} –1.0×10^{3}	1.1 ×10^{2}	11
Photoelectrochemical	1.0×10^{-2}–5.0×10	1.5 ×10^{3}	12
Photoelectrochemical	5.0×10^{-4} –1.0×10	2.9×10^{2}	13
Photoelectrochemical	1.0×10^{-5} – 1.0×10	3.3	This work

17. References

1. G. Mathew, P. Dey , R. Das , S. D. Chowdhury, M. P. Das , P. Veluswamy , B. Neppolian, J. Das, *Biosens. Bioelectron.*, 2018, **115**, 53–60.

2. R. Tang, Y. Chai, X. Liu, L. Li, L. Yang, P. Liu, Y. Zhou ,H. Ju, Y. Cheng, *Biosens. Bioelectron.*, 2018, **117**, 224–231.

3. H. Zhou, T. Han, Q. Wei, S. Zhang, *Anal. Chem.*, 2016, **88**, 2976−2983.

4. S. Zhu, X. Lin, P. Ran, Q. Xia, C. Cheng, Y. J. Ma, Y. Fu, *Biosens. Bioelectron.*, 2017, **91**, 436-440.

5. Q. Wang, Y. F. Ruan, W. W. Zhao, P. Lin, J. J. Xu, and H. Y. Chen, *Anal. Chem.*, 2018, **90**, 3759−3765.

6. T. Edvinsson, R. Soc. open sci., 2018, **5** (9), 180387.

7. B. Zhang, W. Gao, J. Piao, Y. Xiao, B. Wang, W. Peng, X. Gong, Z. Wang, H. Yang, and J. Chang, *ACS Appl. Mater. Inter.*, 2018, **10** (17), 14549-14558.

8. P. Hu, X. Wang, L. Wei, R. Dai, X. Yuan, K. Huang and P. Chen, *J. Mater. Chem. B*, 2019, **7** (31), 4778-4783 .

9. J. T. Cao, Y. L. Wang, J. J. Zhang, Y. X. Dong, F. R. Liu, S. W. Ren, Y. M. Liu, *Anal. Chem.*, 2018, **90** (17), 10334-10339.

10. X. Zheng, L. Li, K. Cui, Y. Zhang, L. Zhang, S. Ge, and J. Yu, *ACS Appl. Mater. Inter.*, 2018, **10** (4), 3333-3340

11. H. Park, G. Han, S. W. Lee, H. Lee, S. H. Jeong, M. Naqi, A. A. AlMutairi, Y. J. Kim, J. Lee, W. Kim, S. Kim, Y. Yoon, and G. Yoo, *ACS Appl. Mater. Inter.*, 2017, **9** (50), 43490-43497

12. H. Chang, H, Kang, E. Ko, B. H. Jun, H. Y. Lee, Y. S. Lee, D. H. Jeong, *ACS Sens.*, 2016, **1** (6), 645-649.

13. S. Lv, K. Zhang, Y. Zeng, D. Tang, *Anal. Chem.*, 2018, **90** (11), 7086-7093.

14. Y. Zang, Y. Ju, J. Jiang, Q. Xu, M. Chu and H. Xue, *Analyst*, 2019, **144**, 4661–4666.